RESEARCH ARTICLE

Electron belt-to-σ-hole switch of noncovalently bound iodine(I) atoms in dithiocarbamate metal complexes†

Lev E. Zelenkov, [iD] [a,b] Anastasiya A. Eliseeva, [iD] [a] Sergey V. Baykov, [iD] [a] Vitalii V. Suslonov, [iD] [a] Bartomeu Galmés, [c] Antonio Frontera, [iD] [c] Vadim Yu. Kukushkin, [iD] [a,d] Daniil M. Ivanov [iD] *[a] and Nadezhda A. Bokach [iD] *[a]

Co-crystallization of dithiocarbamate complexes $[M^{II}(S_2CNEt_2)_2]$ (M = Cu **1**, Ni **2**, Pd **3**, Pt **4**) and 1,3,5-triiodotrifluorobenzene (FIB) gives an isomorphic series of (**1–4**)·2FIB co-crystals exhibiting quadruple Cu/Ni/Pd/Pt isostructural exchange. In the structures of (**1–4**)·2FIB, the halogen-bonded C–I⋯M (Ni, Pd, Pt) and semicoordination M⋯I–C (Cu) metal-involving contacts were identified by X-ray diffractometry and their nature was verified theoretically. The directionality of the $I_{\sigma\text{-hole}}$⋯$d_z^2 M^{II}$ and M^{II}⋯$I_{electron\ belt}$ interactions depends on the identity of a metal center: on going from a rather electrophilic Cu^{II} to substantially more nucleophilic Ni^{II}, Pd^{II}, and Pt^{II} centers, we observed the electron belt-to-σ-hole switch of a noncovalently bound iodine(I) of FIB and, correspondingly, its shift from semicoordination to halogen bonding. The negative values of the electrostatic potentials (given in parentheses) were estimated for all metal centers and they decrease in the order Cu^{II} (−8.8) > Ni^{II} (−24.5) > Pd^{II} (−28.6) > Pt^{II} (−33.3 kcal mol^{-1}). Despite the negative potentials at all M^{II}s, the semicoordinative contact Cu⋯I was established by the recognition of the LP(I) → LP*(Cu) charge transfer using natural bond orbital (NBO) analysis and the comparison of electron density (ED) and electrostatic potential (ESP) minima positions along the I⋯Cu bond paths. In the case of the rather nucleophilic (although positively charged) Pd^{II} and Pt^{II} centers, the contacts C–I⋯d_z^2[Pd] and C–I⋯d_z^2[Pt] can be attributed to the unconventional metal-involving halogen bonding; these contacts are among the strongest (4.30 and 5.42 kcal mol^{-1}, correspondingly) between any metal center and iodine(I)-based σ-hole donors.

1. Introduction

Square-planar metal complexes bearing unhindered and easily accessible metal centers can form several types of metal-involving noncovalent interactions (Fig. 1) including hydrogen bonding (**A**),[1] H–anagostic[2–4] (**A**) and agostic interactions,[5]

[a]Institute of Chemistry, Saint Petersburg State University, Universitetskaya Nab. 7/9, Saint Petersburg, 199034, Russian Federation. E-mail: n.bokach@spbu.ru
[b]Department of Physics and Engineering, ITMO University, Saint Petersburg, 197101, Russian Federation
[c]Department of Chemistry, Universitat de les Illes Balears, Crta de Valldemossa km 7.5, 07122 Palma de Mallorca, Baleares, Spain
[d]Laboratory of Crystal Engineering of Functional Materials, South Ural State University, 76, Lenin Av., Chelyabinsk, 454080, Russian Federation

metallophilic contacts (**B**),[6] semicoordination (**C**),[7] and metal–π interactions (**E**).[8–10]

As far as metal⋯halogen contacts are concerned, noncovalent interactions with halides could be considered as the $M^{\delta+}$⋯$X^{\delta-}$ semicoordination[7] (**C**) owing to the electrophilic nature of most metals in their compounds. In contrast, some rather electron-rich metal centers—such as Rh^I, Ni^{II}, Pd^{II}, Pt^{II}, Au^0, or Au^I—are sufficiently nucleophilic and capable of forming halogen bonding (commonly abbreviated as XB; **D**) interacting with a halogen σ-hole (σh).[11–16] In particular, I_2 forms XBs with Rh^I,[17] Pd^{II},[18] and Pt^{II} metal centers.[19] An iodine center of $R^{EWG}I$ organic species, featuring an electron-withdrawing group (EWG), could also behave as an XB donor and for instance 2-iodopyrazine forms XBs with Ni^{II}, Pd^{II}, and Pt^{II}.[7,20] XB has also been identified in an adduct of tetraiodoethylene with Au^I species[21,22] and co-crystals[23] of iodoform with *trans*-$[M^{II}X_2(\underline{N}CNMe_2)_2]$ (M = Pt, Pd; X = Cl, Br).[11,12] In addition, XB was recognized upon interactions between Ar^FI and gold nanoparticles in water solutions,[24] and RI⋯Au^0 contacts were detected for a gold nanogap.[25,26]

This journal is © the Partner Organisations 2021

Inorg. Chem. Front., 2021, **8**, 2505–2517 | **2505**

Fig. 1 Types of noncovalent interactions involving the metal center in square-planar metal complexes.

Previously we employed neutral square-planar metal complexes with sterically accessible metal sites (bis-dialkylcyanamide halide Pt[II] and Pd[II] complexes,[11–13] Cu[II], Pd[II], and Pt[II] acetylacetonates,[9,10,15,27] and Ni[II] nitrosoguanidinates[7,28]) as XB acceptors toward σh-donating halides. In particular, we revealed the structure-directing role of Ar[F]I···S XB in the construction of supramolecular architectures formed on co-crystallization of the nickel(II) dithiocarbonate [Ni(S$_2$COEt)$_2$] with Ar[F]I.[29] The latter study stimulated our interest in structurally relevant systems and for the continuation of our project we addressed the metal(II) dithiocarbamates [M(S$_2$CNEt$_2$)$_2$] (M = Cu, Ni, Pd, Pt; Fig. 2) and studied their co-crystallization with an Ar[F]I.

In this work, by studying the isostructural co-crystals of [M(S$_2$CNEt$_2$)$_2$] (M = Cu **1**, Ni **2**, Pd **3**, Pt **4**) with 1,3,5-triiodotrifluorobenzene (FIB), we observed a pronounced amphiphilic character of an organoiodine in FIB, which is reflected in different iodine–metal noncovalent bonding patterns. Apart from the expectable two-center C–I···S XBs, the co-crystals featured other structure-directing iodine–metal interactions (Fig. 3). The type of these contacts depends on the nature of metals, which determines electron belt-to-σh switch of noncovalently bound iodine(I) to form either Cu···I–C semicoordination, or metal-involving C–I···$d_{z^2}^2$[M] (M = Ni, Pd, Pt) XB. All our experimental observations accompanied by appropriate theoretical considerations are detailed in sections that follow.

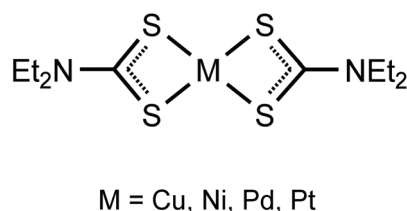M = Cu, Ni, Pd, Pt

Fig. 2 Structures of the parent metal complexes.
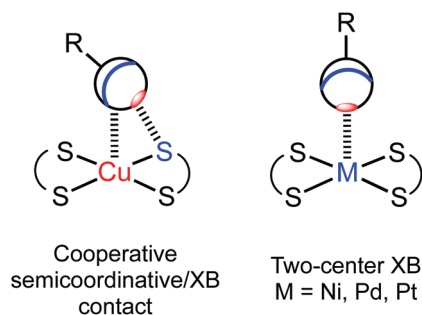
Fig. 3 Types of M···I/I···M interactions identified in this study.

2. Results and discussion

The homoleptic dithiocarbamates [M(S$_2$CNR$_2$)$_2$] (Fig. 2; R = Et) have wide applications in various fields (see the ESI† for the details). Despite this rather broad spectrum of applications, [M(S$_2$CNR$_2$)$_2$] species have never been systematically employed as σh acceptors for crystal engineering involving XBs. The only identified Cl$_2$CH–Cl···S XB including a dithiocarbamate complex has been reported[30] for the X-ray diffraction structure of [Cu[I]{(HO(CH$_2$)$_2$)$_2$NC$\underline{S}_2$}(PPh$_3$)$_2$]·CHCl$_3$. In some other cases, C–Cl···S[14,31–35] and I–I···S[36,37] short contacts with thiocarbamate ligands were considered as "donor-acceptor", "short-contact", or "charge transfer" interactions of the electrostatic nature, but have never been recognized as XB.[38]

The geometrical parameters of R–X···S (X = Cl, Br, I) contacts, including those with dithiocarbamate ligands, retrieved from the Cambridge Crystallographic Database (CSD) are given in the ESI (Table S4†). Notably, S-nucleophilic centers of metal-free dithiocarbamate species functioned as acceptors toward XB,[39–41] coordinative[42] halogen bonding,[43–55] and chalcogen bonding.[56–58]

2.1. Crystallization and common structural motifs of the co-crystals

Complexes **1–4** were co-crystallized with FIB in a 1 : 2 molar ratio in CH$_2$Cl$_2$ at room temperature (RT) to give co-crystals of (**1–4**)·2FIB. Similar cell parameters (Table S1†) and packing features, which are discussed later, indicate that (**1–4**)·2FIB are isomorphic and comprise a family of co-crystals featuring the quadruple Cu/Ni/Pd/Pt isostructural exchange; previously we demonstrated the importance of the dual and triple isostructural exchanges for the design of crystalline materials.[59]

The geometric parameters of the M–S bonds in the co-crystals of the (**1–4**)·2FIB series are different. These distances are similar within 3σ for **1**·2FIB (2.2988(12) and 2.3164(13) Å), **3**·2FIB (2.3280(13) and 2.3325(13) Å), and **4**·2FIB (2.3276(14) and 2.3270(15) Å). In **2**·2FIB (2.2066(14) and 2.2131(14) Å) (Table S2†), the M–S distances are shorter probably because of a smaller covalent Ni[II] radius[60] (1.24 Å) than those of Cu[II] (1.32 Å), Pd[II] (1.39 Å), and Pt[II] (1.36). In all structures, ∠(S–M–S) are smaller than 80° and ∠(S–C–S) (113.4(3) **1**, 109.4(3) **2**, 110.0(3) **3**, 110.1(3)° **4**) are substantially smaller than that in

2506 | *Inorg. Chem. Front.*, 2021, **8**, 2505–2517

This journal is © the Partner Organisations 2021

the uncomplexed $Et_2NCS_2^-$, *e.g.*, 121.69(7)° in the X-ray diffraction structure of $[Ph_4P][S_2CNEt_2]$ (CSD code: BOFRUL).[61] The reduction of ∠(S–C–S) in the metal-bound species can be accounted for by the effect of the ligation on positively charged metal centers that minimize the sulfur–sulfur repulsion.

Parent **2**,[62] **3**,[63] and **4**[64] demonstrate the same geometry around the metal center as in the corresponding co-crystals (**2–4**)·2FIB, while **1** exists as a (**1**)$_2$ dimer[62,65–69] (Fig. 6J) formed by the Cu···S semicoordination.[7] We assume that in co-crystal **1**·2FIB, metal complex **1** does not dimerize because of the stabilization of its monomeric form by the noncovalent interactions (section 2.2).

We carried out the Hirshfeld surface analysis to verify what types of noncovalent forces contribute to the crystal packing in the structures of (**1–4**)·2FIB; for visualization, we used a mapping of the normalized contact distance (d_{norm}) (Fig. 4). The Hirshfeld surface analysis indicates the domination of the contacts involving hydrogen atoms in all cases, specifically H···S (from 21.8 to 23.4%) and H···F hydrogen bonds (from 21.1 to 22.5%), which is expected as the fraction of the H atoms is large (Table S3†). The contribution of I···S and I···M (M = Cu, Ni, Pd, Pt) intermolecular contacts to the Hirshfeld surfaces is also significant and is in the 2.9–3.3% (for I···M) and 8.6–9.1% (for I···S) ranges, respectively. Although the contacts that involve H atoms mainly contribute to the crystal packing, detailed analysis of their geometric characteristics is out of scope of this study, while I···M and I···S interactions are the most interesting in the context of this work and therefore they are consistently discussed in section 2.2.
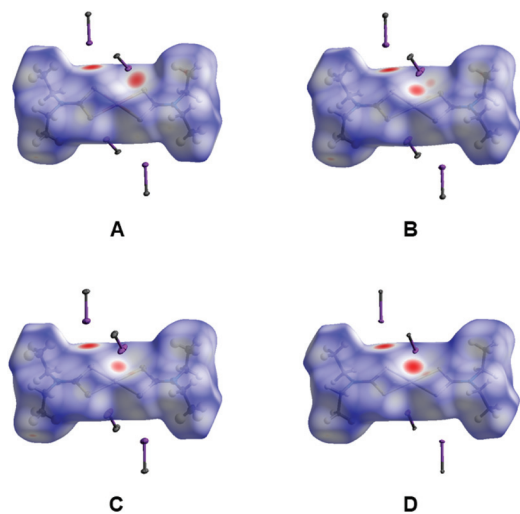

Fig. 4 Hirshfeld surfaces for **1–4** in the X-ray diffraction structures of (**1–4**)·2FIB (A–D, respectively); FIBs are omitted for clarity and only C–I fragments of FIBs are shown. Intermolecular contacts closer than the sum of Bondi vdW radii (Σ_{vdW})[70] highlighted in red, longer contacts are shown in blue, and contacts with a value of approximately Σ_{vdW} are shown in white.

2.2. Noncovalent interactions in the co-crystals

In the structures of (**1–4**)·2FIB, the metal complexes are surrounded by four FIBs (Fig. 5, Table S4†) to form C3S–I2S···S2 two-center XBs and I1S···M/M···I1S contacts, whose nature is different (sections 2.2.1–2.2.3). In **1**·2FIB, the Cu1···I1S interaction is accompanied by the C1S–I1S···S1 contact (section 2.2.4). In the four structures, we detected at least two types of contacts between metal centers and iodine σh (or electron belt) of FIB (Fig. 5). Below in this section we provide arguments supporting our attribution of these contacts.

2.2.1. Simultaneous semicoordinative/XB I···(S–Cu) contact. In **1**·2FIB, we identified the three-center bifurcated C1S–I1S···(S1–Cu1) contact (Fig. 5E and 6I). The C1S–I1S···S1 component belongs to the two-center XB (section 2.2.4), while the nature of the Cu^{II}···I contact is less obvious as the Cu1···I1S distance (3.3924(3) Å) is close to Σ_{vdW} (3.38 Å) and ∠(Cu1···I1S–C1S) 137.06(16)° deviates strongly from 90 or 180°. Although the Cu^{II}···I distance is slightly longer than Σ_{vdW}, the existence of the Cu···I–C interaction in **1**·2FIB, attributed to semicoordination, was confirmed by appropriate theoretical calculations (section 3) and also supported by the literature data. Indeed, copper(II)···iodine semicoordinative contacts shorter than Σ_{vdW} (3.38 Å) are common,[71–77] but examples of Cu^{II}···I contacts longer than Σ_{vdW} are also not unusual[73,74,78–84] (for further details see also the ESI†).

2.2.2. C–I···Ni halogen bonding. In the structure of **2**·2FIB, we identified the C1S–I1S···Ni1 contact (Fig. 5F) belonging to the rare[7] nickel(II)-involving XB. In this linkage, the I1S···Ni1 distance is significantly lower than Σ_{vdW} (3.3388(4) *vs.* 3.61 Å). Although ∠(C1S–I1S···Ni1) 149.1(2)° is less than 150°, this interaction can still be attributed to XB. Indeed, C–I···Nu (Nu = O, N) XBs with such a small angle around an I atom of FIB have been previously reported in CSD structures ODIQAW[85] (149.2(2)°) and MEBXID[7] (148.91(15)°). The I1S···Ni1 contact is accompanied by the I1S···S1 and I1S···S2 short contacts (3.6826(13) and 3.7383(15) *vs.* 3.78 Å, correspondingly). These I···S interactions were confirmed by NCIplot analysis[86,87] (section 3), but the corresponding bond critical points (bond CPs) were not found. Accordingly, we assume that the structure of **2**·2FIB contains the genuine C1S–I1S···Ni1 XB (Fig. 5F and 7K).

Previously we observed the electrophilic–nucleophilic dualism of a nickel(II) center toward its interaction with iodine electron belt (semicoordination) or iodine σh (XB).[7] In most cases, the Ni···I interactions are of semicoordinative nature, and the environment of the nickel(II) center can be viewed as distorted [4 + 2]-octahedral or distorted [4 + 1]-square pyramidal. In the case of the co-crystal [Ni{NHC(NMe$_2$)NN(O)}$_2$]·2FIB, the C–I···Ni interaction is an intermediate between XB and semicoordination as the C–I···Ni angle is 142.51(14)°. Notably, ∠(C1S–I1S···Ni1) (149.1(2)°) in the I1S···Ni1 XB in **2**·2FIB is larger, whereas ∠(Cu1···I1S–C1S) (137.06(16)°) in the Cu1···I1S semicoordination in **1**·2FIB is smaller.

The only known Ni^{II}-involving XB, which is formed between the nickel(II) center and 2-iodopyrazine ligands, was found in [Fe(2-iodopyrazine)(H$_2$O)Ni^{II}(CN)$_4$] MOF[7,20] (Table S5†). In the

This journal is © the Partner Organisations 2021

Inorg. Chem. Front., 2021, **8**, 2505–2517 | **2507**

Fig. 5 C−I⋯S and C−I⋯M interactions in (**1**−**4**)·2FIB (**E**−**H**, respectively); FIBs are omitted for clarity and only C−I fragments of FIBs are shown. The contacts shorter than Σ_{vdW} and with confirmed bond critical points (section 3) given by dotted lines. Thermal ellipsoids are shown with 50% probability.

Fig. 6 C−I⋯(S−Cu) contact in the structure of **1**·2FIB (**I**) and the dimerization of [Cu^{II}(S$_2$CNR$_2$)$_2$] (**J**) *via* Cu^{II}⋯S semicoordination.
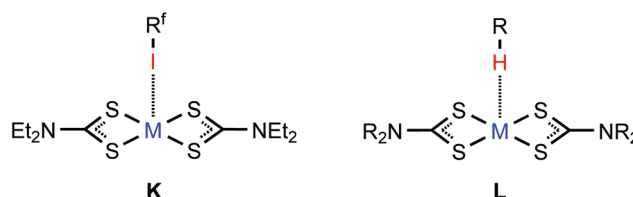
Fig. 7 C−I⋯M^{II} (M = Ni, Pd, Pt) XB in (**2**−**4**)·2FIB (**K**) and the C−H⋯M^{II} hydrogen bonding in the structure of [M^{II}(S$_2$CNR$_2$)$_2$] (**L**).

structure of **2**·2FIB, the C−I⋯Ni XB (3.3388(4) Å) is even shorter than that in [Fe(2-iodopyrazine)(H$_2$O)Ni^{II}(CN)$_4$] (d(I⋯Ni^{II}) 3.4702(17) Å) and one nickel(II) center forms two XBs. This unprecedentedly high nucleophilicity of the Ni^{II} center is probably due to the strong σ-donation of the four

dithiocarbamate S atoms (see additional comments in the ESI†).

2.2.3. C−I⋯Pd halogen bonding. In the structures of Pd^{II}-based co-crystal **3**·2FIB and Pt^{II}-based co-crystal **4**·2FIB (section 2.2.4), co-crystal metal-involving contacts are also attributed to

2508 | *Inorg. Chem. Front.*, 2021, **8**, 2505–2517

This journal is © the Partner Organisations 2021

XB. In **3·2FIB**, we recognized the C1S–I1S···Pd1 metal-involving contact (Fig. 5G and 7K) belonging to XB as the I1S···Pd1 distance (3.3732(4) Å is substantially less than Σ_{vdW} (3.61 Å) and ∠(C1S–I1S···Pd1) 153.0(2)° tends to 180°. In **3·2FIB**, we observed the C1S–I1S···Pd1 interaction accompanied by the C1S–I1S···S2 short contact (3.7221(14) *vs.* 3.78 Å). While the existence of the latter was supported by NCIPlot analysis, the corresponding bond CP was not detected (section 3). Based on these theoretical data we attribute the C1S–I1S···Pd1 contact to two-center XB.

Similar to the nickel(ɪɪ) center in the structure of **2·2FIB**, the palladium(ɪɪ) atom in **3·2FIB** can also form both Pd^{II}···I semicoordination bonds and I···Pd^{II} XB (Table S5†). The Pd^{II}···I semicoordination has previously been identified for cationic and neutral palladium(ɪɪ) complexes, featuring P- or S-donating ligands.[88–92] Simultaneous Pd^{II}···I semicoordination and I···Pd^{II} XB have been found for the structure of [Pd(μ-SCH$_2$CO$_2$Me)$_2$]$_8$·I$_2$.[18] This co-crystal demonstrates the shortest I···Pd^{II} XB (3.0953(6) Å and 3.1021(6) Å; Table S5†) and the formation of the strong XB is accounted for by the deep σh of I$_2$ and the inclusion character of the co-crystal (see the ESI† for a more detailed discussion of the data collected in Table S5†).

The nucleophilicity of the metal center in **3·2FIB** is relevant to the previously reported C–H···Pd^{II} hydrogen bonding (Fig. 7L) observed in some [Pd(S$_2$CNR$_2$)$_2$] crystals[4,93,94] and also to the polarized metallophilic interactions M$^{\delta+}$···Pd$^{\delta-}$ (M^I = Cu^I, Ag^I) involving [Pd(S$_2$CNR$_2$)$_2$] entities.[95–97]

2.2.4. C–I···Pt halogen bonding. The structure of platinum(ɪɪ)-based co-crystal **4·2FIB** (Fig. 5H and 7K) exhibits the C1S–I1S···Pt1 metal-involving XB (3.3351(4) *vs.* 3.73 Å), while ∠(C1S–I1S···Pt1) 160.1(2)° is rather close to 180°. Similar to the structures of (**2–3**)·2FIB, the C1S–I1S···S2 contact was also found (3.6931(16) *vs.* 3.78 Å) and confirmed (section 3) by NCIPlot analysis, but the I···S bond CP was not observed. The C1S–I1S···Pt1 XB is stronger than that in **3·2FIB** in the absolute (3.3351(4) Å for Pt *vs.* 3.3732(4) Å for Pd) and relative ($R_{Bondi} = d$(I1S···Pt1)/$\Sigma_{vdW} = 0.89$ *vs.* $R_{Bondi} = d$(I1S···Pd1)/$\Sigma_{vdW} = 0.93$) values. These data are in line with the previously reported data for the isostructural co-crystals *trans*-[MCl$_2$(NCNMe$_2$)$_2$]·2CHX$_3$ (M = Pd, Pt; X = Br, I), where the C–X···Pt^{II} (X = Br, I) XB are shorter and stronger than the C–X···Pd^{II} (X = Br, I) interactions.[12]

The Pt^{II}···I semicoordination is known,[98–101] but it is significantly less common than I···Pt^{II} XBs. All reported C–I···Pt^{II} bonds (Table S5†), apart from the very strong coordinative I–I···Pt^{II} XBs,[19,102–104] are weaker than that in **4·2FIB** (3.3351(4) Å) thus indicating the strong donating effect of the dithiocarbamate ligands.

The Pt^{II} nucleophilicity found for **4·2FIB** is in line with the C–H···Pt^{II} hydrogen bonding (Fig. 7L) identified for [Pt(S$_2$CNR$_2$)$_2$] species[93,94] and it is also coherent with the polarized M$^{\delta+}$···Pt$^{\delta-}$ (M^I = Cu^I, Ag^I) metallophilic interactions.[95–97]

2.2.5. Two-center I···S XB. In the structures of (**1–4**)·2FIB, the I2S···S2 distances (3.3929(13)–3.4161(15) Å) and ∠(C3S–I2S···S2) (163.87(16)–169.01(13)°) (Table S4†) are almost the same and these values are in agreement with the IUPAC distance and angle criteria for XB.[38]

The R–I···S–Ni XBs have been reported for the related structures of [Ni(S$_2$COEt)$_2$]·2FIB and [Ni(S$_2$COEt)$_2$]·2(1,4-diiodotetrafluorobenzene).[29] Although the R–I···S–M (M = Cu^{II},[105] Ni^{II},[106] and Pd^{II} (ref. 107)) short contacts were earlier recognized, their XB nature was not considered. The XB between FIB and an S-nucleophile has been also reported[108] for co-crystals formed between an XB donor and thiocyanates in [Et$_4$N]SCN and [^{n}Bu$_4$N]SCN. These C–I···SCN$^-$ (3.2447(7)–3.2881(7) Å) interactions are shorter than the corresponding R–I···S–M distances (3.3929(13)–3.4161(15) Å) probably because of the anionic nature of SCN$^-$.

In **1·2FIB**, I1S···S1 interaction is not independent as it is accompanied by the Cu1···I1S interaction (section 2.2.1). For (**2–4**)·2FIB, the I1S···S1 and I1S···S2 contacts were also found (sections 2.2.2–2.2.4), but the corresponding bond CPs were not detected (section 3). Notably, the existence of a metal-involving bifurcate C–(μ$_2$-I)···(M–Nu) can be postulated upon analysis of appropriate geometric criteria of this entity. However, to reliably confirm its existence, an additional computational study (including Bader's analysis) is required. Indeed, in some similar cases the calculations verified only one CP between iodine and metal centers and this disproved the initial hypothesis on the bifurcate binding.[15,16,109]

3. Theoretical studies

First, we computed the molecular electrostatic potential (MEP) of compounds **1–4** in order to rationalize the XB interactions and the nucleophilic nature of the metal centers and the S-atoms of the ligands, since both atoms function as an XB acceptor in the co-crystals. The MEP surfaces are given in Fig. S2† for **1–4** and in Fig. S1† for the FIB molecule that shows the typical σh at the I-atom. The MEP results gathered in Fig. S2† evidence that the Cu-atom has a very modest nucleophilic character in **1** (−8.8 kcal mol^{-1}). The negative value over the metal center is likely due to the strong electron donation of the thiocarbamate ligands. Although the relevant [Ni(S$_2$COEt)$_2$] complex also demonstrates a low negative potential on the metal center (−11.0 kcal mol^{-1}), it forms the Ni^{II}···S semicoordination, which was identified in the co-crystals [Ni(S$_2$COEt)$_2$]·2FIB and [Ni(S$_2$COEt)$_2$]·2(1,4-diiodotetrafluorobenzene).[29] The MEP minimum in **1** is located at the coordinated S-atoms (−26.0 kcal mol^{-1}). The rest of the compounds exhibit larger values of MEP at the M^{II}-centers (ranging from −24.5 to −33.3 kcal mol^{-1}), increasing on going from **2** to **4**. Interestingly for the Pt complex (**4**), the MEP minimum is located at the metal center instead of the S-atom, thus evidencing the strong XB acceptor ability of Pt. This MEP analysis strongly agrees with the directionality of the C–I···M XB interactions in the co-crystals. For instance, in the **1·2FIB** co-crystal, the C–I···Cu angle is 137.1° (the C–I points to the S atom) and in the **4·2FIB** co-crystal, the C–I···Pt angle increases to 160°. In fact, a strong linear relationship ($r = 0.988$) has been found between the C–I···M^{II} angle and the MEP value at the metal center (Fig. S3†). This remarkable relationship demonstrates

This journal is © the Partner Organisations 2021

Inorg. Chem. Front., 2021, **8**, 2505–2517 | **2509**

that the directionality of the interaction is affected by the nucleophilicity of the metal center.

The energetic features of the two types of XBs observed in the structures of the co-crystals have been analyzed using DFT calculations and also characterized by a combination of the quantum theory of "atoms in molecules" (QTAIM) and noncovalent interaction plot (NCIPlot)[86,87] computational tools for the (**1–4**)·FIB isolated clusters of two types, both extracted from the corresponding X-ray diffraction data. Fig. 8 shows the results for the C–I···S interaction in the four model clusters reported herein revealing that they are energetically similar, varying from −5.9 to −6.3 kcal mol^{-1}. The strength of the interaction increases from **1**·FIB to **4**·FIB, in agreement with the MEP values at the S atoms that become more negative on moving from **1** to **4**. The combined QTAIM/NCIplot analysis shows that the XB is characterized by a bond CP, bond path interconnecting the I and S atoms. It is further characterized by a bluish NCIPlot isosurface, thus evidencing its attractive and moderately strong nature. Moreover, it also reveals the existence of ancillary C–H···I hydrogen bonds also characterized by a bond CP and bond path interconnecting the H-atom to the negative belt of the I-atom. The color of the NCIplot isosurface for this H-bond is green, thus anticipating a weaker interaction. This is confirmed by the contribution of each interaction that has been evaluated using the potential energy density at the bond CPs (the data are summarized in

Table S7†). It can be observed that the contribution of the C–H···I H-bond is less than 1 kcal mol^{-1} in all cases.

Fig. 9 shows a similar analysis of the C–I···M^{II} interaction in four other (**1–4**)·FIB isolated clusters. The binding energies (see Table S7†) in this series of metal complexes show that platinum(II) is the best XB acceptor in line with the MEP results.

It is interesting to highlight the differences between the C–I···Cu/Ni and C–I···Pd/Pt interactions in terms of the NCIplot analysis. That is, in latter metal complexes the isosurface is blue (or even dark blue in Pt) between the C–I bond and the metal center and green between the C–I bond and the S-atoms of the thiocarbamate ligand, showing that the I···M interaction dominates over the I···S one. In contrast, the interaction in the **1**·FIB cluster is characterized by bluish isosurfaces between the I and both the Cu and S-atoms. In fact, for **1**·FIB the QTAIM analysis shows two bond CPs and bond paths connecting the I-atom to the Cu and S-atoms. Moreover, the value of the charge density (ρ) at the bond CP that connects the I to the S atom is similar to the CP that connects the I to the Cu-atom (see Table S8† for details), thus confirming their equivalent importance. This result is inconsistent with the MEP surface that showed a very small MEP value at the Cu-atom and a much larger value at the S-atom. This suggests that apart from the small electrostatic attraction between the positive σh at the I-atom the negative MEP over the Cu-atom, an additional con-

Fig. 8 Combined QTAIM and NCIplot surface analyses of the **1**·FIB (a), **2**·FIB (b), **3**·FIB (c), and **4**·FIB (d) model clusters extracted from the X-ray coordinates. Bond and ring CPs are represented using red and yellow spheres, respectively. The color scale for the NCIplot is −0.03 < sign(λ_2)ρ < 0.03.
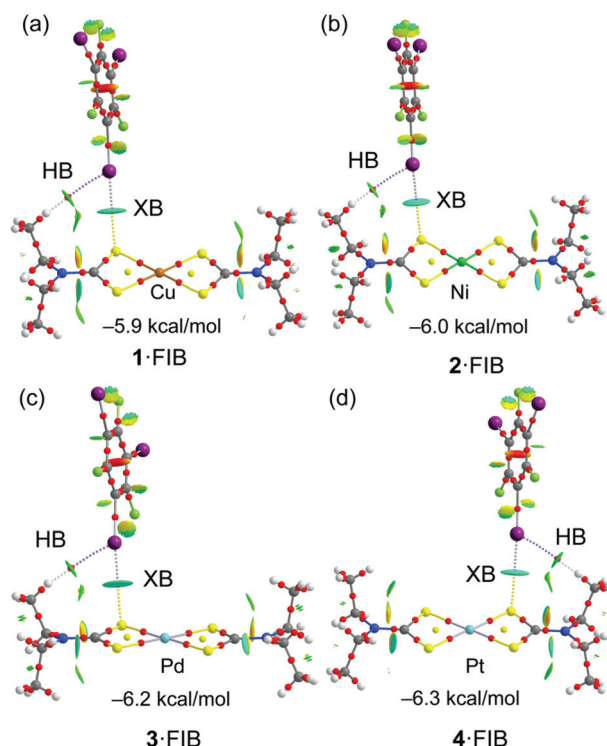

Fig. 9 Combined QTAIM and NCIplot surface analyses of **1**·FIB (a), **2**·FIB (b), **3**·FIB (c), and **4**·FIB (d) model clusters extracted from the X-ray coordinates. Bond and ring CPs are represented using red and yellow spheres, respectively. The color scale for the NCIplot is −0.03 < sign(λ_2)ρ < 0.03.
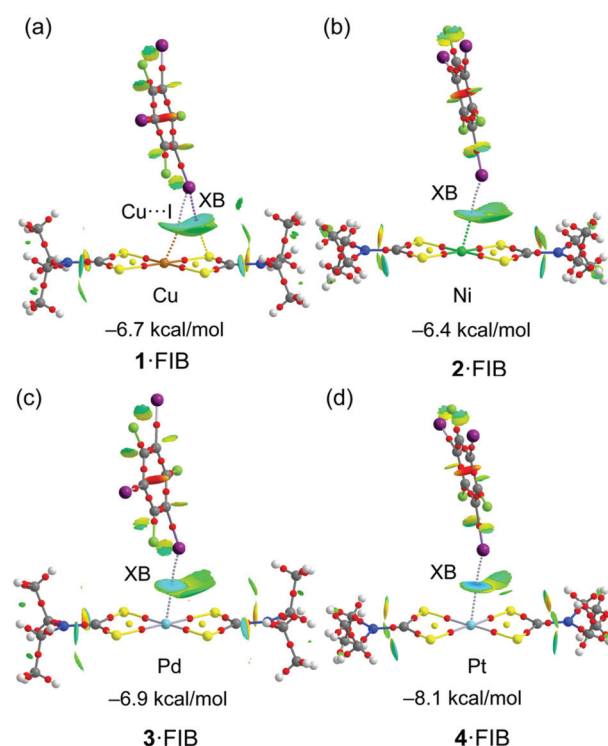
tribution must exist, which can be tentatively assigned to a semicoordination bond, as proposed above. To verify this hypothesis, the Natural Bonding Orbital analysis has been used (see "Computational details" in the ESI†). The orbital donor–acceptor interactions have been examined in terms of the second order perturbation analysis. Agreeably, it reveals an electron donation from the LP at the I-atom to the unfilled $4p_z$ orbital of the Cu atom [(LP(I) → LP*(Cu)] with a concomitant stabilization energy of $E^{(2)} = 3.85$ kcal mol^{-1}. Quite remarkably this stabilization energy is very similar to the dissociation energy estimated using the V_r predictor for this particular contact (3.32 kcal mol^{-1}; Table S8†) and supports the semicoordination character of the I···Cu contact.

In the case of **2**·FIB, although only one bond CP and bond path connect the I to the Ni atom, the NCIPlot shows an extended isosurface with bluish color embracing the I atom and both the Ni and S-atoms, thus suggesting a similar participation of both atoms as electron donors. In fact, the MEP values are large and negative at both the Ni and S-atoms. The QTAIM parameters are gathered in Table S8† revealing some interesting issues. First, in **1**·FIB, the energies associated with C–I···S and C–I···Cu contacts are similar and the sum of both contributions (6.54 kcal mol^{-1}) is similar to the dimerization energy shown in Fig. 9 (−5.9 kcal mol^{-1}). Second, the energy associated with the I···M^{II} contact derived from V_r increases on going from **1**·FIB to **4**·FIB (from 3.32 kcal mol^{-1} for Cu to 5.42 kcal mol^{-1} for Pt). The difference from the dimerization energies is included in Fig. 9 and those summarized in Table S8† for co-crystals (**2–4**)·FIB can be associated with the stabilization energy due to the I···S interaction that is also important (as revealed by the NCIplot) in spite of the absence of the corresponding bond CP and bond path connecting the I to the S-atom. Finally, we also examined the existence of the orbital donor–acceptor interaction described above for **1**·FIB for the rest of the metal complexes. Interestingly, only in the case of cluster **2**·FIB, a similar LP(I) → $4p_z$(Ni) electron donation is observed with a concomitant stabilization energy of $E^{(2)} = 1.30$ kcal mol^{-1}. It is smaller than that obtained for the Cu cluster and also smaller than the dissociation energy estimated for the I···Ni contact using the V_r predictor (3.91 kcal mol^{-1}; Table S8†). This suggests that the Ni···I interaction has a dual character (semicoordination and XB).

More information on atom philicities in the I···M interactions can be obtained by two additional methods. According to the first scheme, previously used by us,[110] one should compare the positions of bond paths and areas of electron localization function (ELF), corresponding to lone pairs and σh.[13,111] For this purpose, the ELF projections with the plotted bond path and CPs (Fig. S4†) were drawn along the S···S···I planes containing metal nuclear CPs. In **1**·FIB, the I···S bond path passes through the area with ELF > 0.75 on the S atom (which corresponds to the region of lone electron pairs) and through the area with the depleted ELF region on I atoms (corresponding to the reduced shielding of I nuclei in the σh); inspection of these data confirms the XB nature of the I···S interaction. At the same time, the relevant Cu···I bond path passes through the I area with the ELF value that is larger than that for the I···S bond path, and the consideration of these values could indicate the nucleophilicity of the I atom toward the Cu center.

In (**2–4**)·FIB, the I···M (M = Ni, Pd, Pt) bond paths pass through the depleted ELF region on the I atoms (σh), and this observation confirms the electrophilic nature of iodine atoms when they interact with the metal centers. ELF projections in all clusters allow the identification of the ELF areas, corresponding to the d^9- or d^8-level, around the metal centers. The enlargement of these ELF areas in a row Cu < Ni < Pd < Pt is probably associated with the increase of the nucleophilicity of the metal centers. The enlargement and also the ELF depletion on the I atoms in the same row can also be illustrated by 1D ELF projections along the I···M bond paths (Fig. 10).

Nevertheless, any bond path corresponding to noncovalent interactions with the metal centers passes through this area, because any d^8- or d^9-square-planar metal-involving interaction has to be far from the ligands in the metal complex plane. Therefore, another method to verify the philicities should be applied. The analysis of the order of the electron density (ED) and electrostatic potential (ESP) minima along the bond path[21,53–55,57–59] is useful for these purposes. The minimum of ESP is shifted toward the nucleophilic atom, while the ED minimum is shifted toward the electrophilic atom.

The 1D profiles of the ED and ESP functions along the I···M bond paths are depicted in Fig. 11. For **1**·FIB, the ED minimum is slightly shifted to the Cu nucleus, whereas the ESP minimum is closer to the I nucleus. It means that the Cu atom functions as an electrophile, while the I center acts as a nucleophile, and the Cu···I interaction should be treated as the semicoordination. This observation is in accordance with the Natural Bonding Orbital analysis data (see above), which indicate the LP(I) → LP*(Cu) charge transfer.

The opposite situation was found for the projections in (**2–4**)·FIB, where the ESP minima are closer to a metal center and the ED minima are near the I atom. To summarize this part, we confirmed the nucleophilicity of Ni, Pd, and Pt toward I in all three cases, and proved that the C–I···M (M = Ni, Pd, Pt) interactions belong to the category of metal-involving XBs.

Fig. 10 ELF projections along the I···M bond paths.

This journal is © the Partner Organisations 2021

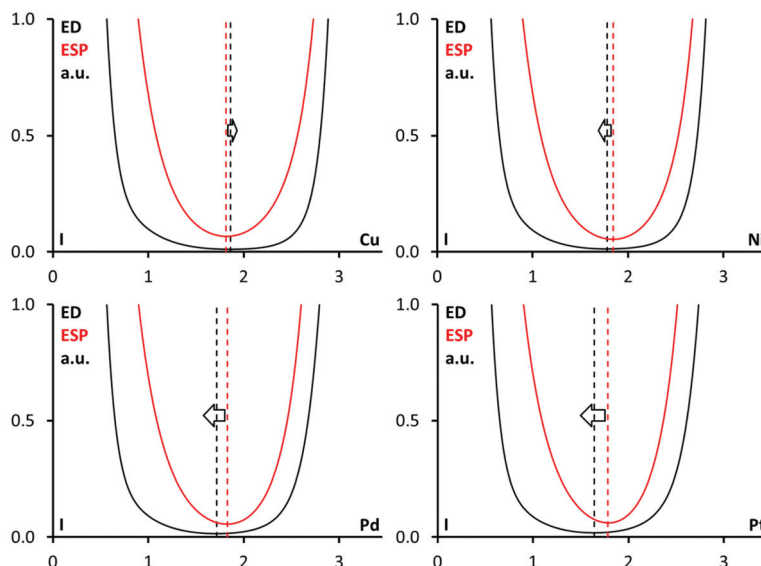*Inorg. Chem. Front.*, 2021, **8**, 2505–2517 | **2511**

Fig. 11 Criterion ED minimum *vs.* ESP minimum: the ED (black) and the ESP (red) for the I⋯M interactions; interatomic distances are in Å.

Taken together, the DFT study evidences a progressive change from semicoordination M⋯I to XB on going from **1**·FIB to **4**·FIB species, where **2**·FIB demonstrates the LP(I) → LP*(Ni) charge transfer, but the C–I⋯Ni interaction is already an XB according to ED and ESP positions along the I⋯Ni bond path.

4. Conclusions

The co-crystallization of FIB with the metal(II) dithiocarbamates $[M(S_2CNEt_2)_2]$ (**1–4**; M = Cu, Ni, Pd, Pt) gave an isostructural series of co-crystals (**1–4**)·2FIB, where the noncovalent interactions such as I⋯S XB and C–I⋯M/M⋯I–C metal-involving contacts were detected by X-ray diffraction and their existence was confirmed theoretically. Crystal packing motifs in all these isomorphic co-crystals are similar and one can conclude that the difference in the directionality of I⋯M/M⋯I interactions depends on the identity of a metal center. The linear correlation between the C–I⋯M^{II} angle and MEP values on the metals reflects the switch in the I⋯M/M⋯I interaction patterns on going from Ni^{II} to Cu^{II}. The C–I⋯M^{II} angle is the smallest for the rather electrophilic Cu^{II} and gradually increases in the row Cu^{II} > Ni^{II} > Pd^{II} > Pt^{II} along with the increase of the nucleophilicity of these metal centers. According to the change in the nature of the metal center, the electron belt-to-σh switch of noncovalently bound iodine(I) occurs, which demonstrates the amphiphilic character of an organoiodine in FIB. In the Cu^{II} > Ni^{II} > Pd^{II} > Pt^{II} row, the electron localization function around the metal centers is also gradually increased reflecting the growth of diffuseness of the *d*-sublevel and therefore the growth of the nucleophilicity.

In the case of a rather electrophilic copper(II), the semicoordinative nature of the Cu⋯I contact was established by the recognition of the LP(I) → LP*(Cu) charge transfer using NBO analysis and the comparison of ED and ESP minima positions

along the I⋯Cu bond paths. At a glance, a negative value of the electrostatic potential at the metal center in $[Cu(S_2CNEt_2)_2]$ (−8.8 kcal mol⁻¹) contradicts the electrophilic character of copper(II). However, we demonstrated[29] that the semicoordination is still possible when a metal center exhibits a negative potential. The nature of the semicoordination contact in the co-crystal of $[Cu(S_2CNEt_2)_2]$ can be rationalized by orbital, rather than electrostatic effects.[29]

In **2·2FIB**, the nickel(II) center (which in principle can exhibit electrophilic-nucleophilic dualism[7]) demonstrates LP(I) → LP*(Ni) charge transfer as confirmed by the NBO analysis. At the same time, analysis of ED and ESP minima positions along the I⋯Ni bond paths indicates the nucleophilicity of the Ni^{II} center. Pronounced negative potential at the nickel(II) atom in $[Ni(S_2CNEt_2)_2]$ (−24.5 kcal mol⁻¹), in comparison with that of the copper(II) atom in $[Cu(S_2CNEt_2)_2]$, additionally proves the nucleophilicity of the Ni^{II} center.

In the case of even more nucleophilic palladium(II) and platinum(II) (potentials at the metal centers for $[M(S_2CNEt_2)_2]$ are 28.6 and −33.3 kcal mol⁻¹, correspondingly), contacts C–I⋯Pd and C–I⋯Pt can be attributed to metal-involving XB. These contacts are among the strongest XB (4.30 and 5.42 kcal mol⁻¹, correspondingly) between these metal centers and iodine(I)-based electrophiles. We believe that the observed C–I⋯Pd metal-involving XB interaction should be taken into account upon further studies focused on fine mechanisms of palladium-catalyzed reactions that include the oxidative addition step of aryl iodides.[12]

Author contributions

L. E. Zelenkov – conceptualization and investigation; A. A. Eliseeva – investigation; S. V. Baykov – investigation; V. V. Suslonov – investigation; B. Galmés – computational

2512 | *Inorg. Chem. Front.*, 2021, **8**, 2505–2517

This journal is © the Partner Organisations 2021

study; A. Frontera – computational study and writing; V. Yu. Kukushkin – conceptualization and writing; D. M. Ivanov – conceptualization, methodology, and writing; N. A. Bokach – methodology, writing, and project administration.

Conflicts of interest

There are no conflicts to declare.

Acknowledgements

References

1 D. S. Bolotin, V. K. Burianova, A. S. Novikov, M. Y. Demakova, C. Pretorius, P. P. Mokolokolo, A. Roodt, N. A. Bokach, V. V. Suslonov, A. P. Zhdanov, K. Y. Zhizhin, N. T. Kuznetsov and V. Y. Kukushkin, Nucleophilicity of Oximes Based upon Addition to a Nitrilium closo-Decaborate Cluster, *Organometallics*, 2016, **35**, 3612–3623.

2 H. V. Huynh, L. R. Wong and P. S. Ng, Anagostic Interactions and Catalytic Activities of Sterically Bulky Benzannulated N-Heterocyclic Carbene Complexes of Nickel(II), *Organometallics*, 2008, **27**, 2231–2237.

3 A. B. d. Oliveira, J. Beck, S. E. B. S. Mellone and J. Daniels, A new example of intramolecular C-H...Ni anagostic interactions: synthesis, crystal structure and Hirshfeld analysis of cis-bis[4-methyl-2-(1,2,3,4-tetrahydronaphthalen-1-ylidene)hydrazinecarbothioamidato-[kappa]2N1,S]nickel(II) dimethylformamide monosolvate, *Acta Crystallogr., Sect. E: Crystallogr. Commun.*, 2017, **73**, 859–863.

4 M. K. Yadav, G. Rajput, L. B. Prasad, M. G. B. Drew and N. Singh, Rare intermolecular M...H–C anagostic interactions in homoleptic Ni(ii)–Pd(ii) dithiocarbamate complexes, *New J. Chem.*, 2015, **39**, 5493–5499.

5 V. N. Mikhaylov, V. N. Sorokoumov, K. A. Korvinson, A. S. Novikov and I. A. Balova, Synthesis and Simple Immobilization of Palladium(II) Acyclic Diaminocarbene Complexes on Polystyrene Support as Efficient Catalysts for Sonogashira and Suzuki–Miyaura Cross-Coupling, *Organometallics*, 2016, **35**, 1684–1697.

6 A. N. Chernyshev, M. V. Chernysheva, P. Hirva, V. Y. Kukushkin and M. Haukka, Weak aurophilic inter-

actions in a series of Au(III) double salts, *Dalton Trans.*, 2015, **44**, 14523–14531.

7 Z. M. Bikbaeva, D. M. Ivanov, A. S. Novikov, I. V. Ananyev, N. A. Bokach and V. Y. Kukushkin, Electrophilic–Nucleophilic Dualism of Nickel(II) toward Ni⋯I Noncovalent Interactions: Semicoordination of Iodine Centers via Electron Belt and Halogen Bonding via σ-Hole, *Inorg. Chem.*, 2017, **56**, 13562–13578.

8 E. R. T. Tiekink, Supramolecular assembly based on "emerging" intermolecular interactions of particular interest to coordination chemists, *Coord. Chem. Rev.*, 2017, **345**, 209–228.

9 A. V. Rozhkov, M. A. Krykova, D. M. Ivanov, A. S. Novikov, A. A. Sinelshchikova, M. V. Volostnykh, M. A. Konovalov, M. S. Grigoriev, Y. G. Gorbunova and V. Y. Kukushkin, Reverse Arene Sandwich Structures Based upon π-Hole⋯[M^{II}] (d^8M=Pt, Pd) Interactions, where Positively Charged Metal Centers Play the Role of a Nucleophile, *Angew. Chem., Int. Ed.*, 2019, **58**, 4164–4168.

10 S. V. Baykov, S. I. Filimonov, A. V. Rozhkov, A. S. Novikov, I. V. Ananyev, D. M. Ivanov and V. Y. Kukushkin, Reverse Sandwich Structures from Interplay between Lone Pair−π-Hole Atom-Directed C⋯d_z^2[M] and Halogen Bond Interactions, *Cryst. Growth Des.*, 2020, **20**, 995–1008.

11 D. M. Ivanov, A. S. Novikov, I. V. Ananyev, Y. V. Kirina and V. Y. Kukushkin, Halogen bonding between metal centers and halocarbons, *Chem. Commun.*, 2016, **52**, 5565–5568.

12 S. V. Baykov, U. Dabranskaya, D. M. Ivanov, A. S. Novikov and V. P. Boyarskiy, Pt/Pd and I/Br Isostructural Exchange Provides Formation of C–I⋯Pd, C–Br⋯Pt, and C–Br⋯Pd Metal-Involving Halogen Bonding, *Cryst. Growth Des.*, 2018, **18**, 5973–5980.

13 U. Dabranskaya, D. M. Ivanov, A. S. Novikov, Y. V. Matveychuk, N. A. Bokach and V. Y. Kukushkin, Metal-Involving Bifurcated Halogen Bonding C–Br⋯η^2(Cl–Pt), *Cryst. Growth Des.*, 2019, **19**, 1364–1376.

14 R. Reyes-Martínez, R. Mejia-Huicochea, J. A. Guerrero-Alvarez, H. Höpfl and H. Tlahuext, Synthesis, heteronuclear NMR and X-ray crystallographic studies of two dinuclear diorganotin(IV) dithiocarbamate macrocycles, *ARKIVOC*, 2008, **2008**, 19–30.

15 A. V. Rozhkov, D. M. Ivanov, A. S. Novikov, I. V. Ananyev, N. A. Bokach and V. Y. Kukushkin, Metal-involving halogen bond Ar–I⋯[d_z^2Pt^{II}] in a platinum acetylacetonate complex, *CrystEngComm*, 2020, **22**, 554–563.

16 E. A. Katlenok, A. V. Rozhkov, O. V. Levin, M. Haukka, M. L. Kuznetsov and V. Y. Kukushkin, Halogen Bonding Involving Palladium(II) as an XB Acceptor, *Cryst. Growth Des.*, 2021, **21**(2), 1159–1177.

17 D. W. Shaffer, S. A. Ryken, R. A. Zarkesh and A. F. Heyduk, Ligand Effects on the Oxidative Addition of Halogens to (dpp-nacnacR)Rh(phdi), *Inorg. Chem.*, 2012, **51**, 12122–12131.

18 Y. Yamashina, Y. Kataoka and Y. Ura, Inclusion of an Iodine Molecule in a Tiara-Like Octanuclear Palladium Thiolate Complex, *Eur. J. Inorg. Chem.*, 2014, **2014**, 4073–4078.

This journal is © the Partner Organisations 2021

Inorg. Chem. Front., 2021, **8**, 2505–2517 | **2513**

19 R. A. Gossage, A. D. Ryabov, A. L. Spek, D. J. Stufkens, J. A. M. van Beek, R. van Eldik and G. van Koten, Models for the Initial Stages of Oxidative Addition. Synthesis, Characterization, and Mechanistic Investigation of η^1-I^2 Organometallic "Pincer" Complexes of Platinum. X-ray Crystal Structures of $[PtI(C_6H_3\{CH_2NMe_2\}_2\text{-}2,6)(\eta^1\text{-}I_2)]$ and exo-meso-$[Pt(\eta^1\text{-}I_3)(\eta^1\text{-}I_2)(C_6H_3\{CH_2N(t\text{-}Bu)Me\}_2\text{-}2,6)]$, *J. Am. Chem. Soc.*, 1999, **121**, 2488–2497.

20 O. I. Kucheriv, S. I. Shylin, V. Ksenofontov, S. Dechert, M. Haukka, I. O. Fritsky and I. A. Gural'skiy, Spin Crossover in Fe(II)–M(II) Cyanoheterobimetallic Frameworks (M = Ni, Pd, Pt) with 2-Substituted Pyrazines, *Inorg. Chem.*, 2016, **55**, 4906–4914.

21 H. M. Yamamoto, J.-I. Yamaura and R. Kato, Multicomponent Molecular Conductors with Supramolecular Assembly: Iodine-Containing Neutral Molecules as Building Blocks, *J. Am. Chem. Soc.*, 1998, **120**, 5905–5913.

22 I. S. Aliyarova, D. M. Ivanov, N. S. Soldatova, A. S. Novikov, P. S. Postnikov, M. S. Yusubov and V. Y. Kukushkin, Bifurcated Halogen Bonding Involving Diaryliodonium Cations as Iodine(III)-Based Double-σ-Hole Donors, *Cryst. Growth Des.*, 2021, **21**(2), 1136–1147.

23 Co-crystals: Preparation, Characterization and Applications, in *Monographs in Supramolecular Chemistry*, ed. C. B. Aakeröy and A. S. Sinha, Royal Society of Chemistry, 2020, https://pubs.rsc.org/en/content/ebook/978-1-78801-115-0.

24 I. Blakey, Z. Merican, L. Rintoul, Y.-M. Chuang, K. S. Jack and A. S. Micallef, Interactions of iodoperfluorobenzene compounds with gold nanoparticles, *Phys. Chem. Chem. Phys.*, 2012, **14**, 3604–3611.

25 Y. Komoto, S. Fujii, K. Hara and M. Kiguchi, Single Molecular Bridging of Au Nanogap Using Aryl Halide Molecules, *J. Phys. Chem. C*, 2013, **117**, 24277–24282.

26 L.-L. Peng, B. Huang, Q. Zou, Z.-W. Hong, J.-F. Zheng, Y. Shao, Z.-J. Niu, X.-S. Zhou, H.-J. Xie and W. Chen, Low Tunneling Decay of Iodine-Terminated Alkane Single-Molecule Junctions, *Nanoscale Res. Lett.*, 2018, **13**, 121.

27 A. V. Rozhkov, A. S. Novikov, D. M. Ivanov, D. S. Bolotin, N. A. Bokach and V. Y. Kukushkin, Structure-Directing Weak Interactions with 1,4-Diiodotetrafluorobenzene Convert One-Dimensional Arrays of $[M^{II}(acac)_2]$ Species into Three-Dimensional Networks, *Cryst. Growth Des.*, 2018, **18**, 3626–3636.

28 Z. M. Bikbaeva, A. S. Novikov, V. V. Suslonov, N. A. Bokach and V. Y. Kukushkin, Metal-mediated reactions between dialkylcyanamides and acetamidoxime generate unusual (nitrosoguanidinate)nickel(II) complexes, *Dalton Trans.*, 2017, **46**, 10090–10101.

29 L. E. Zelenkov, D. M. Ivanov, E. K. Sadykov, N. A. Bokach, B. Galmés, A. Frontera and V. Y. Kukushkin, Semicoordination Bond Breaking and Halogen Bond Making Change the Supramolecular Architecture of Metal-Containing Aggregates, *Cryst. Growth Des.*, 2020, **20**(10), 6956–6965.

30 S. L. Tan, C. I. Yeo, P. J. Heard, G. R. Akien, N. R. Halcovitch and E. R. T. Tiekink, [N,N-Bis(2-hydroxyethyl)dithiocarbamato-[kappa]2S,S']bis(triphenylphosphane-[kappa]P)copper(I) chloroform monosolvate: crystal structure, Hirshfeld surface analysis and solution NMR measurements, *Acta Crystallogr., Sect. E: Crystallogr. Commun.*, 2016, **72**, 1799–1805.

31 A. Torres-Huerta, H. Höpfl, H. Tlahuext, I. F. Hernández-Ahuactzi, M. Sánchez, R. Reyes-Martínez and D. Morales-Morales, Dinuclear Macrocyclic Palladium Dithiocarbamates Derived from the Homologous Series of Aliphatic 1,x-Diamines (x = 4–10), *Eur. J. Inorg. Chem.*, 2013, **2013**, 61–69.

32 K. Himoto, T. Horii, S. Oda, S. Suzuki, K. Sugimoto, T. Okubo, M. Maekawa and T. Kuroda-Sowa, Crystal structure of a new mixed-metal coordination polymer consisting of NiII piperidine-dithiocarbamate and pentanuclear CuI-I cluster units, *Acta Crystallogr., Sect. E: Crystallogr. Commun.*, 2018, **74**, 233–236.

33 O. V. Loseva and A. V. Ivanov, Interaction of binuclear zinc diethyldithiocarbamate with $H[AuCl_4]$/2M HCl: The preparation, supramolecular self-organization, and thermal behavior of the heteropolynuclear complex $([Au\{S_2CN(C_2H_5)_2\}_2]_2[ZnCl_4]\cdot1/2CO(CH_3)_2\cdot1/2CHCl_3)_n$, *Russ. J. Inorg. Chem.*, 2014, **59**, 1491–1500.

34 I. A. Lutsenko, A. V. Ivanov, E. V. Korneeva and A. I. Tursina, Host-guest supramolecular complexes of the composition $[M\{NH(CH2)4O\}\{S2CN(C2H5)2\}2]$ · CHCl3 (M = Zn, 63Cu(II)): Synthesis, structure, spectral properties, and thermal behavior, *Russ. J. Coord. Chem.*, 2012, **38**, 709–716.

35 I. A. Lutsenko, E. V. Korneeva and A. V. Ivanov, Supramolecular complexes $[M\{NH(CH_2)_4O\}\{S_2CN(C_2H_5)_2\}_2]\cdot$ CCl4 (M = Zn or ^{63}Cu(II)): Synthesis, structures, spectral and thermal properties, *Russ. J. Coord. Chem.*, 2016, **42**, 494–501.

36 N. V. Khitrich, I. I. Seifullina, S. E. Nefedov and A. V. Mazepa, Interaction between N,N,N′,N′-tetramethylthiuram disulfide and cobalt(II) salts: Dependence of the product composition and structure on the nature of the anion, *Russ. J. Inorg. Chem.*, 2006, **51**, 1000–1008.

37 C. L. Raston, A. H. White, D. Petridis and D. Taylor, Crystal structure of tris(NN-diethyldithiocarbamato)iron(IV) pentaiodide, *J. Chem. Soc., Dalton Trans.*, 1980, 1928–1931.

38 G. R. Desiraju, P. S. Ho, L. Kloo, A. C. Legon, R. Marquardt, P. Metrangolo, P. Politzer, G. Resnati and K. Rissanen, Definition of the halogen bond (IUPAC Recommendations 2013), *Pure Appl. Chem.*, 2013, **85**, 1711.

39 V. A. Ivolgina, M. S. Chernov'yants, L. D. Popov, V. V. Suslonov, G. S. Borodkin, N. V. Luanguzov and N. A. Avtushenko, Perspective anti-thyroid drug 2-thioxo-5-(3,4,5-trimethoxybenzylidene) thiazolidin-4-one: X-ray and thermogravimetric characterization of two novel molecular adducts, obtained by interaction with I2, *J. Mol. Struct.*, 2019, **1180**, 629–635.

40 Y. Le Gal, D. Lorcy, O. Jeannin, F. Barrière, V. Dorcet, J. Lieffrig and M. Fourmigué, C=S...I halogen bonding interactions in crystalline iodinated dithiole-2-thiones and thiazole-2-thiones, *CrystEngComm*, 2016, **18**, 5474–5481.

2514 | *Inorg. Chem. Front.*, 2021, **8**, 2505–2517

This journal is © the Partner Organisations 2021

41 J. S. Casas, M. V. Castaño, M. D. Couce, A. Sánchez, J. Sordo, M. D. Torres, S. A. Vázquez and E. M. Vázquez-López, Relevance of weak intermolecular forces on the supramolecular structure of free or DMSO solvated 5-(4-X-benzylidene)rhodanines (X = F, Cl, Br, I), *J. Mol. Struct.*, 2016, **1120**, 100–114.

42 L. Koskinen, P. Hirva, E. Kalenius, S. Jääskeläinen, K. Rissanen and M. Haukka, Halogen bonds with coordinative nature: halogen bonding in a S–I⁺–S iodonium complex, *CrystEngComm*, 2015, **17**, 1231–1236.

43 F. Demartin, F. A. Devillanova, A. Garau, F. Isaia, V. Lippolis and G. Verani, Reactions of N-methylbenzothiazole-2(3H)-thione (1) and -selone (2) with ICl: Synthesis and X-ray crystal structures of the charge-transfer adducts 1·ICl (I) and 2·ICl (II), *Polyhedron*, 1999, **18**, 3107–3113.

44 V. Daga, S. K. Hadjikakou, N. Hadjiliadis, M. Kubicki, J. H. Z. dos Santos and I. S. Butler, Synthesis, Spectroscopic and Structural Characterization of Novel Diiodine Adducts with the Heterocyclic Thioamides, Thiazolidine-2-thione (tzdtH), Benzothiazole-2-thione (bztzdtH) and Benzimidazole-2-thione (bzimtH), *Eur. J. Inorg. Chem.*, 2002, **2002**, 1718–1728.

45 C. D. Antoniadis, G. J. Corban, S. K. Hadjikakou, N. Hadjiliadis, M. Kubicki, S. Warner and I. S. Butler, Synthesis and Characterization of (PTU)I2 (PTU = 6-n-propyl-2-thiouracil) and (CMBZT)I2 (CMBZT = 5-chloro-2-mercaptobenzothiazole) and Possible Implications for the Mechanism of Action of Anti-Thyroid Drugs, *Eur. J. Inorg. Chem.*, 2003, **2003**, 1635–1640.

46 G. J. Corban, S. K. Hadjikakou, N. Hadjiliadis, M. Kubicki, E. R. T. Tiekink, I. S. Butler, E. Drougas and A. M. Kosmas, Synthesis, Structural Characterization, and Computational Studies of Novel Diiodine Adducts with the Heterocyclic Thioamides N-Methylbenzothiazole-2-thione and Benzimidazole-2-thione: Implications with the Mechanism of Action of Antithyroid Drugs, *Inorg. Chem.*, 2005, **44**, 8617–8627.

47 I.-E. Parigoridi, G. J. Corban, S. K. Hadjikakou, N. Hadjiliadis, N. Kourkoumelis, G. Kostakis, V. Psycharis, C. P. Raptopoulou and M. Kubicki, Structural motifs of diiodine complexes with amides and thioamides, *Dalton Trans.*, 2008, 5159–5165.

48 A. Tamilselvi and G. Mugesh, Interaction of heterocyclic thiols/thiones eliminated from cephalosporins with iodine and its biological implications, *Bioorg. Med. Chem. Lett.*, 2010, **20**, 3692–3697.

49 M. C. Aragoni, M. Arca, F. Demartin, F. A. Devillanova, T. Gelbrich, A. Garau, M. B. Hursthouse, F. Isaia and V. Lippolis, Charge-Transfer Adducts of N-Methylthiazolidine-2-thione with IBr and I2: An Example of Polymorphism Featuring Interpenetrating Three-Dimensional Subcomponent Assemblies and Halogen···π···Halogen Weak Interactions, *Cryst. Growth Des.*, 2007, **7**, 1284–1290.

50 G. J. Corban, C. D. Antoniadis, S. K. Hadjikakou, N. Kourkoumelis, V. Y. Tyurin, A. Dolgano, E. R. Milaeva, M. Kubicki, P. V. Bernhardt, E. R. T. Tiekink, S. Skoulika and N. Hadjiliadis, Reactivity of di-iodine toward thiol: Desulfuration reaction of 5-nitro-2-mercapto-benzimidazole upon reaction with di-iodine, *Heteroat. Chem.*, 2012, **23**, 498–511.

51 L. Koskinen, P. Hirva, A. Hasu, S. Jääskeläinen, J. Koivistoinen, M. Pettersson and M. Haukka, Modification of the supramolecular structure of [(thione)IY] (Y = Cl, Br) systems by cooperation of strong halogen bonds and hydrogen bonds, *CrystEngComm*, 2015, **17**, 2718–2727.

52 L. Koskinen, S. Jääskeläinen, P. Hirva and M. Haukka, Tunable Interaction Strength and Nature of the S···Br Halogen Bonds in [(Thione)Br2] Systems, *Cryst. Growth Des.*, 2015, **15**, 1160–1167.

53 E. Kotali, A. Varvoglis, A. Bozopoulos and P. Rentzeperis, A stable dibenzoiodolyl pyrrolidinedithiocarbamate, *J. Chem. Soc., Chem. Commun.*, 1985, 1819–1820.

54 A. P. Bozopoulos and P. J. Rentzeperis, Structure of (2,2-biphenylylene)(1-pyrrolidinecarbodithioato)iodine(III) chloroform solvate, *Acta Crystallogr., Sect. C: Cryst. Struct. Commun.*, 1986, **42**, 1014–1016.

55 A. P. Bozopoulos and P. J. Rentzeperis, Structure of [bis(p-methoxyphenyl)](diethylaminocarbodithioato)iodine(III), *Acta Crystallogr., Sect. C: Cryst. Struct. Commun.*, 1987, **43**, 914–916.

56 V. P. Fedin, M. N. Sokolov, O. A. Geras'ko, A. V. Virovets, N. V. Podberezskaya and V. Y. Fedorov, Triangular M3Se74+ and M3Se44+ complexes (M = Mo, W). An X-ray study of Mo3Se7(Et2NCS2)4 and W3Se7(Et2NCS2)4, *Inorg. Chim. Acta*, 1991, **187**, 81–90.

57 H.-P. Zhu, C.-N. Chen, Q.-T. Liu and J.-T. Chen, A Triangular [Mo3S7]4+ Complex: Tris(diethyldithiocarbamato-S,S')tris([mu]2-[eta]2-disulfido)([mu]3-sulfido)trimolybdenum(IV)(3 Mo-Mo)Diethyldithiocarbamate, *Acta Crystallogr., Sect. C: Cryst. Struct. Commun.*, 1998, **54**, 1273–1275.

58 K. G. Myakishev, T. M. Polyanskaya and E. A. Il'inchik, SYNTHESIS AND STRUCTURE OF THE COMPLEX {MO3 (μ3-S)(μ2-S2) 3[(C2H5)2NCS2] 3} + [(C2H5)2NCS 2]-, *Russ. J. Gen. Chem.*, 2000, **70**, 1489–1493.

59 A. V. Buldakov, M. A. Kinzhalov, M. A. Kryukova, D. M. Ivanov, A. S. Novikov, A. S. Smirnov, G. L. Starova, N. A. Bokach and V. Y. Kukushkin, Isomorphous Series of PdII-Containing Halogen-Bond Donors Exhibiting Cl/Br/I Triple Halogen Isostructural Exchange, *Cryst. Growth Des.*, 2020, **20**, 1975–1984.

60 B. Cordero, V. Gómez, A. E. Platero-Prats, M. Revés, J. Echeverría, E. Cremades, F. Barragán and S. Alvarez, Covalent radii revisited, *Dalton Trans.*, 2008, 2832–2838, DOI: 10.1039/B801115J.

61 C. M. Donahue, I. K. Black, S. L. Pecnik, T. R. Savage, B. L. Scott and S. R. Daly, Synthesis, characterization and structural comparisons of phosphonium and arsenic dithiocarbamates with alkyl and phenyl substituents, *Polyhedron*, 2014, **75**, 110–117.

This journal is © the Partner Organisations 2021

Inorg. Chem. Front., 2021, **8**, 2505–2517 | **2515**

62 B. Cvek, V. Milacic, J. Taraba and Q. P. Dou, Ni(II), Cu(II), and Zn(II) Diethyldithiocarbamate Complexes Show Various Activities Against the Proteasome in Breast Cancer Cells, *J. Med. Chem.*, 2008, **51**, 6256–6258.

63 P. P. Phadnis, V. K. Jain, T. Schurr, A. Klein, F. Lissner, T. Schleid and W. Kaim, Synthesis, spectroscopy, structure and photophysical properties of dinaphthylmethylarsine complexes of palladium(II) and platinum(II), *Inorg. Chim. Acta*, 2005, **358**, 2609–2617.

64 A. Baker and M. Emett, The Crystal and Molecular Structures of Bis(diethyldithiocarbamato)platinum(II) and Bis[di(2-hydroxyethyl)dithiocarbamato]platinum(II), *Aust. J. Chem.*, 1992, **45**, 429–434.

65 M. Bonamico, G. Dessy, A. Mugnoli, A. Vaciago and L. Zambonelli, Structural studies of metal dithiocarbamates. II. The crystal and molecular structure of copper diethyldithiocarbamate, *Acta Crystallogr.*, 1965, **19**, 886–897.

66 B. H. O'Connor and E. N. Maslen, A second analysis of the crystal structure of copper(II) diethyldithiocarbamate, *Acta Crystallogr.*, 1966, **21**, 828–830.

67 F. Jian, Z. Wang, Z. Bai, X. You, H.-K. Fun, K. Chinnakali and I. A. Razak, The crystal structure, equilibrium and spectroscopic studies of bis(dialkyldithiocarbamate) copper(II) complexes [Cu2(R2dtc)4] (dtc=dithiocarbamate), *Polyhedron*, 1999, **18**, 3401–3406.

68 S. K. Verma, R. Kadu and V. K. Singh, A Facile Synthesis, Crystallographic, Spectral, Thermal, and Electrochemical Investigations of Neutral [Cu2(Et2dtc)4] Dimer, *Synth. React. Inorg., Met.-Org., Nano-Met. Chem.*, 2014, **44**, 441–448.

69 C. Wang, J. Niu, J. Li and X. Ma, Synthesis, structures and properties of three copper complexes with dibutyldithiocarbamate ligand, *J. Mol. Struct.*, 2017, **1135**, 75–81.

70 A. Bondi, van der Waals Volumes and Radii, *J. Phys. Chem.*, 1964, **68**, 441–451.

71 S. Youngme, C. Chailuecha, G. A. van Albada, C. Pakawatchai, N. Chaichit and J. Reedijk, Synthesis, crystal structure, spectroscopic and magnetic properties of doubly and triply bridged dinuclear copper(II) compounds containing di-2-pyridylamine as a ligand, *Inorg. Chim. Acta*, 2004, **357**, 2532–2542.

72 S. Indoria, T. S. Lobana, D. Singh, S. Kumari, P. Kumari, T. Bala, A. Kamal, A. K. Jassal, I. García Santos, A. Castineiras and J. P. Jasinski, Stabilization of CuII–I Bonds Using 2-Benzoylpyridine Thiosemicarbazones – Synthesis, Structure, Spectroscopy, Fluorescence, and Cyclic Voltammetry, *Eur. J. Inorg. Chem.*, 2015, **2015**, 5106–5117.

73 S. Jana, S. Bhowmik, K. Harms, A. Bauzá, A. Frontera and S. Chattopadhyay, Theoretical study on the degree of delocalization of unpaired spin in two mixed valence copper (II/I) complexes with isomeric chelating diamines and iodide, *Inorg. Chim. Acta*, 2016, **451**, 16–22.

74 H.-H. Li, J.-B. Li, M. Wang, S.-W. Huang and Z.-R. Chen, Two Neutral Heterometallic Iodoargentate Hybrid Frameworks: Structures and Properties, *J. Cluster Sci.*, 2011, **22**, 573–586.

75 S. Zhang, Y. Cao, H. Zhang, X. Chai, Y. Chen and R. Sun, Influence of synthesis condition on product formation: hydrothermal auto-oxidated synthesis of five copper halides with ratio of Cu(I)/Cu(II) in 1:1, 2:1, 3:1, 4:1 and 1:0, *J. Solid State Chem.*, 2008, **181**, 3327–3336.

76 A. A. Mohamed, S. Ricci, A. Burini, R. Galassi, C. Santini, G. M. Chiarella, D. Y. Melgarejo and J. P. Fackler, Halide and Nitrite Recognizing Hexanuclear Metallacycle Copper(II) Pyrazolates, *Inorg. Chem.*, 2011, **50**, 1014–1020.

77 S. Herres, A. J. Heuwing, U. Flörke, J. Schneider and G. Henkel, Hydroxylation of a methyl group: synthesis of [Cu2(btmmO)2I]+ and of [Cu2(btmmO)2]2+ containing the novel ligand {bis(trimethylmethoxy)guanidino} propane (btmmO) by copper-assisted oxygen activation, *Inorg. Chim. Acta*, 2005, **358**, 1089–1095.

78 B. Freckmann and K.-F. Tebbe, Die Kristallstruktur des Bis (1,2-diaminoethan)-kupfer(II)-diiodocuprats (I), [Cu(H2NCH2CH2NH2)2(CuI4/2)2] / The Crystal Structure of [Cu(H2NCH2CH2NH2)2(CuI4/2)2], *Z. Naturforsch. B*, 1980, **35**, 1319.

79 K.-F. Tebbe and S. Nafepour, Tetra(N-methylimidazol)-kupfer(II)-bis(triiodid) [Cu(C4H6N2)4](I3)2, *Acta Crystallogr., Sect. C: Cryst. Struct. Commun.*, 1994, **50**, 171–173.

80 J. Ballester, O. J. Parker and G. L. Breneman, Structure of tetrakis(imidazole)copper(II) diiodide, *Acta Crystallogr., Sect. C: Cryst. Struct. Commun.*, 1993, **49**, 1421–1424.

81 Y. Yang, Z.-Q. Zhang, J.-M. Ding, S.-M. Wang and Y.-C. Ju, Crystal structure of tetrapyridinecopper(II) bis(triiodide), [Cu(C5H5N)4][I3]2, *Z. Kristallogr. – New Cryst. Struct.*, 2011, **226**, 185.

82 I. K. Thomassen, H. Vazquez-Lima, K. J. Gagnon and A. Ghosh, Octaiodoporphyrin, *Inorg. Chem.*, 2015, **54**, 11493–11497.

83 M. Aryaeifar, H. A. Rudbari and G. Bruno, A close insight into the nature of intra- and intermolecular interactions in new Cu(II) Schiff base complexes derived from halogenated salicylaldehydes and allylamine: Theoretical and crystallographic studies, *Polyhedron*, 2018, **155**, 114–128.

84 X.-P. Zhou, D. Li, S.-L. Zheng, X. Zhang and T. Wu, Cu(I) or Cu(I)−Cu(II) Mixed-Valence Complexes of 2,4,6-Tri(2-pyridyl)-1,3,5-triazine: Syntheses, Structures, and Theoretical Study of the Hydrolytic Reaction Mechanism, *Inorg. Chem.*, 2006, **45**, 7119–7125.

85 A. Carletta, M. Zbačnik, M. Vitković, N. Tumanov, V. Stilinović, J. Wouters and D. Cinčić, Halogen-bonded cocrystals of N-salicylidene Schiff bases and iodoperfluorinated benzenes: hydroxyl oxygen as a halogen bond acceptor, *CrystEngComm*, 2018, **20**, 5332–5339.

86 E. R. Johnson, S. Keinan, P. Mori-Sánchez, J. Contreras-García, A. J. Cohen and W. Yang, Revealing Noncovalent Interactions, *J. Am. Chem. Soc.*, 2010, **132**, 6498–6506.

87 J. Contreras-García, E. R. Johnson, S. Keinan, R. Chaudret, J.-P. Piquemal, D. N. Beratan and W. Yang, NCIPLOT: A Program for Plotting Noncovalent Interaction Regions, *J. Chem. Theor. Comput.*, 2011, **7**, 625–632.

2516 | *Inorg. Chem. Front.*, 2021, **8**, 2505–2517

This journal is © the Partner Organisations 2021

88 N. A. Bailey and R. Mason, Crystal and molecular structures of two crystallographic modifications of trans-diiodobis(dimethylphenylphosphine)palladium(II), *J. Chem. Soc. A*, 1968, 2594–2605.

89 A. J. Blake, W.-S. Li, V. Lippolis, S. Parsons and M. Schroder, Dichloro([mu]-[18]aneN2S4)dipalladium(II) Bis(triiodide), *Acta Crystallogr., Sect. C: Cryst. Struct. Commun.*, 1998, **54**, 1408–1410.

90 A. M. M. Meij, S. Otto and A. Roodt, Synthesis and characterisation of palladium(II) iodo complexes containing water soluble phosphine ligands. Crystal structures of [PdI2(PTA-H)2][PtI3(PTA)]2·2H$_2$O and trans-[PdI2(PTA)2], *Inorg. Chim. Acta*, 2005, **358**, 1005–1011.

91 M. Tsutomu, N. Koji, A. Shizuka and M. Katsuhiko, Interaction Modes with a Halide Anion of Metal Centers of Edge-Sharing Dinuclear Complexes Bearing a Bent Form, *Bull. Chem. Soc. Jpn.*, 2002, **75**, 1547–1552.

92 E. Doxiadi, R. Vilar, A. J. P. White and D. J. Williams, Anion-templated synthesis and structural characterisation of Ni/Pd-containing metalla-macrocycles, *Polyhedron*, 2003, **22**, 2991–2998.

93 A. N. Gupta, V. Kumar, V. Singh, K. K. Manar, M. G. B. Drew and N. Singh, Intermolecular anagostic interactions in group 10 metal dithiocarbamates, *CrystEngComm*, 2014, **16**, 9299–9307.

94 S. Poirier, F. Rahmani and C. Reber, Large d–d luminescence energy variations in square-planar bis(dithiocarbamate) platinum(II) and palladium(II) complexes with near-identical MS4 motifs: a variable-pressure study, *Dalton Trans.*, 2017, **46**, 5279–5287.

95 M. Ebihara, K. Tokoro, M. Maeda, M. Ogami, K. Imaeda, K. Sakurai, H. Masuda and T. Kawamura, Bonding interaction between Group 10 and 11 metals. Synthesis, structure and properties of [M3(S2CNR2)6M′2]2+ (M = Pt or Pd; M′ = Ag or Cu; R = Et, Pri, Prn, Bun or C6H11), *J. Chem. Soc., Dalton Trans.*, 1994, 3621–3635.

96 E. Masahiro, S. Kenji, K. Takashi, K. Hiroaki, M. Hideki and T. Tooru, Covalent Bonding of Two Ag(I) Atoms to a Square-Planar Pt(II) Atom in [Pt3(S2CNEt2)6Ag2](ClO4)2, *Chem. Lett.*, 1990, **19**, 415–418.

97 M. Ebihara, K. Tokoro, K. Imaeda, K. Sakurai, H. Masuda and T. Kawamura, Complexes of silver(I) with bis(dialkyldithiocarbamato)platinum(II) as ligand: synthesis and structures of [Pt3(S2CNPri2)6Ag2](BF4)2 and [Pt3(S2CNBun2)6Ag2](ClO4)2, *J. Chem. Soc., Chem. Commun.*, 1992, 1591–1592.

98 N. C. Stephenson, The crystal structure of di-iododi-(o-phenylenebisdimethylarsine) platinum(II) Pt(C6H4[As (CH3)2]2)2I2, *J. Inorg. Nucl. Chem.*, 1962, **24**, 791–795.

99 R. Contreras, M. Valderrama, A. Nettle and D. Boys, Synthesis and characterization of new homo-heterobinuclear platinum(II) complexes with dimethylphosphonate as bridging ligands. Crystal structure of [(η2dppm)Pt{μ-P(O) (OMe)2}2 (μ-I)PtMe3], *J. Organomet. Chem.*, 1997, **527**, 125–132.

100 T. Tanase, H. Toda and Y. Yamamoto, Incorporation of Group 11 Metal Ions into a Diplatinum Center Leading to Pt$_2$M Heterotrinuclear Complexes Supported by a Tridentate Phosphine Ligand (M = Au, Ag, Cu), *Inorg. Chem.*, 1997, **36**, 1571–1577.

101 S. Otto and A. Roodt, Five co-ordination at platinum(II) in a water soluble tertiary phosphine complex: crystal structure of [Pt(PTA)3(I)2]·CH3OH, *Inorg. Chem. Commun.*, 2001, **4**, 49–52.

102 J. A. M. Van Beek, G. Van Koten, W. J. J. Smeets and A. L. Spek, Model for the initial stage in the oxidative addition of I2 to organoplatinum(II) compounds. X-ray structure of square-pyramidal [PtIII{C6H3(CH2NMe2)2-o, o'}(.eta.1-I2)] containing a linear Pt-I-I arrangement, *J. Am. Chem. Soc.*, 1986, **108**, 5010–5011.

103 J. A. M. van Beek, G. van Koten, G. P. C. M. Dekker, E. Wissing, M. C. Zoutberg and C. H. Stam, Synthesis and reactivity towards diiodine of palladium(II) and platinum (II) complexes with non-cyclic and cyclic ligands (C6H3 {CH2NR1R2}2–2,6)−. End-on diiodine-platinum(II) bonding in macrocyclic [PtI(C6H3{CH2NMe(CH2)7MeNCH2}-2,6)(η1-I2)], *J. Organomet. Chem.*, 1990, **394**, 659–678.

104 L. S. von Chrzanowski, M. Lutz, A. L. Spek, B. M. J. M. Suijkerbuijk and R. J. M. Klein Gebbink, {2,6-Bis[[(dimethylamino-[kappa]N)methyl]-4-{[(2,5-dioxo-1-pyrrolidinyl)oxy]carbonyl}phenyl-[kappa]C1}(diiodine)iodido-platinum(II) dichloromethane hemisolvate, *Acta Crystallogr., Sect. E*, 2007, **63**, m1223–m1225.

105 X. M. Ren, Z. P. Ni, S. Noro, T. Akutagawa, S. Nishihara, T. Nakamura, Y. X. Sui and Y. Song, Diversities of Coordination Geometry at Cu^{2+} Center in the Bis(maleonitriledithiolato)cuprate Complexes: Syntheses, Magnetic Properties, X-ray Crystal Structural Analyses, and DFT Calculations, *Cryst. Growth Des.*, 2006, **6**, 2530–2537.

106 H. Zhou and X.-M. Ren, Bis[1-(4-iodobenzyl)pyridinium] bis(maleonitriledithiolato)nickelate(II), *Acta Crystallogr., Sect. E: Struct. Rep. Online*, 2007, **63**, m1932.

107 W. B. Heuer and W. H. Pearson, Synthesis and characterization of nickel-group bis(dithiocroconate) complexes and dicyanomethylene-substituted analogues, *J. Chem. Soc., Dalton Trans.*, 1996, 3507–3513, DOI: 10.1039/DT9960003507.

108 P. Cauliez, V. Polo, T. Roisnel, R. Llusar and M. Fourmigué, The thiocyanate anion as a polydentate halogen bond acceptor, *CrystEngComm*, 2010, **12**, 558–566.

109 E. A. Katlenok, M. Haukka, O. V. Levin, A. Frontera and V. Y. Kukushkin, Supramolecular Assembly of Metal Complexes by (Aryl)I···d[Pt^{II}] Halogen Bonds, *Chem. – Eur. J.*, 2020, **26**, 7692–7701.

110 M. Bulatova, D. M. Ivanov and M. Haukka, Classics Meet Classics: Theoretical and Experimental Studies of Halogen Bonding in Adducts of Platinum(II) 1,5-Cyclooctadiene Halide Complexes with Diiodine, Iodoform, and 1,4-Diiodotetrafluorobenzene, *Cryst. Growth Des.*, 2021, **21**(2), 974–987.

111 A. Savin, R. Nesper, S. Wengert and T. F. Fässler, ELF: The Electron Localization Function, *Angew. Chem., Int. Ed. Engl.*, 1997, **36**, 1808–1832.

This journal is © the Partner Organisations 2021

Inorg. Chem. Front., 2021, **8**, 2505–2517 | **2517**